Hafnium-neodymium isotope evidence for enhanced weathering and uplift-climate interactions during the Late Cretaceous

Pauline Corentin, Emmanuelle Pucéat, Pierre Pellenard, Nicolas Freslon, Michel Guiraud, Justine Blondet, Thierry Adatte, Germain Bayon

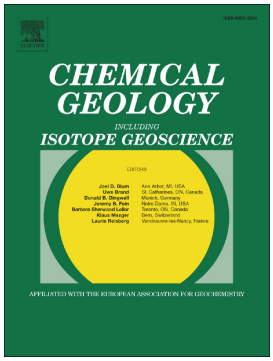

Hafnium-neodymium isotope evidence for enhanced weathering and uplift-climate interactions during the Late Cretaceous

Pauline Corentin, Emmanuelle Pucéat, Pierre Pellenard, Nicolas Freslon, Michel Guiraud, Justine Blondet, Thierry Adatte, Germain Bayon

PII: S0009-2541(22)00018-3

DOI: https://doi.org/10.1016/j.chemgeo.2022.120724

Reference: CHEMGE 120724

To appear in: *Chemical Geology*

Received date: 5 May 2021

Revised date: 22 December 2021

Accepted date: 10 January 2022

Please cite this article as: P. Corentin, E. Pucéat, P. Pellenard, et al., Hafnium-neodymium isotope evidence for enhanced weathering and uplift-climate interactions during the Late Cretaceous, *Chemical Geology* (2021), https://doi.org/10.1016/j.chemgeo.2022.120724

Hafnium-neodymium isotope evidence for enhanced weathering and uplift-climate interactions during the Late Cretaceous

Pauline Corentin[1*], Emmanuelle Pucéat[1], Pierre Pellenard[1], Nicolas Freslon[1,2], Michel Guiraud[1], Justine Blondet[1], Thierry Adatte[3], Germain Bayon[4]

[1]Biogéosciences, UMR 6282 CNRS, Université Bourgogne Franche-Comté, 21000 Dijon, France

[2] ISTO - Université d'Orléans, CNRS, BRGM, UMR 7327, F-45071, Orléans, France

[3]Institute of Earth Sciences, Géopolis, University of Lausanne, Lausanne, Switzerland

[4]IFREMER, Unité de Recherche Géosciences Marines, F-29280 Plouzané, France

*Corresponding author : pauline.corentin@u-bourgogne.fr, Biogéosciences, UMR 6282 CNRS, Université Bourgogne Franche-Comté, 6 bvd Gabriel, 21000 Dijon, France.

Abstract

The processes initiating the first cooling step of the last greenhouse-to-icehouse transition, from 90 million years ago (Ma) onward still remain enigmatic. While the combination of mountain uplift and continental weathering has been proposed as a major sink for atmospheric CO_2 and a climate driver over geological timescales, this hypothesis is much debated and its potential importance in triggering the late Cretaceous global cooling is yet to be explored. In this work, we combined clay mineralogy, trace and major element concentrations, and a new proxy of silicate weathering intensity based on Nd and Hf isotopes ($\Delta\varepsilon_{Hf(t)clay}$) to explore the potential links between the uplift of the brazilian margin, silicate weathering and climate evolution during the late Cretaceous. Our new $\Delta\varepsilon_{Hf(t)clay}$ proxy data suggest - for the first time - that marked increase of silicate weathering intensity occurred in southeast Brazil during the late Cretaceous, from ~ 85 to 70 Ma, related to the tectonic uplift affecting the eastern South American margin at that time. Combined with clay mineralogical

analyses, our Hf-Nd isotope data further suggests the existence of a relatively arid local climate during the Turonian-Santonian interval, during which physical disaggregation of rocks most likely prevailed, accompanying the uplift of the Brazilian margin. From the Santonian, we propose that the exposure of new high-elevation regions favoured instead locally enhanced precipitations and more hydrolysing conditions, thereby promoting chemical weathering and atmospheric CO_2 drawdown. Altogether, our multi-proxy investigation suggests that the uplift of the Brazilian margin could have contributed to the late Cretaceous cooling, potentially playing a key role in the onset of the last greenhouse-to-icehouse transition.

Keywords: Paleoclimate – Tectonic-climate interaction – Isotope geochemistry – Clay mineralogy – Brazilian margin.

1. Introduction

The late Cretaceous period experienced a pronounced long-term cooling marking the very first step of the last greenhouse to icehouse transition, which culminated at the Eocene/Oligocene boundary (ca. 33 Ma) with the onset of icehouse climate conditions (Friedrich et al., 2012; O'Brien et al., 2017). Understanding the processes that drove global cooling at that time is fundamental as they may still contribute to maintain our modern climate into this mode. The late Cretaceous long-term cooling was accompanied by a decrease in atmospheric CO_2 levels (pCO_2), hence implying a close connection with the long-term carbon cycle (Royer, 2010). Over million-year timescales, the global carbon cycle is governed by atmospheric CO_2 inputs from mid-ocean ridges, large igneous provinces (LIPs) and continental arc volcanic activity, and CO_2 consumption related to continental silicate weathering and preservation of organic matter (Berner et al., 1983; McKenzie et al., 2016).

While a reduction in mantle CO_2 outgassing likely contributed to the observed pCO_2 decrease during this period (McKenzie et al., 2016), the occurrence of a major uplift phase in South America at that time, extending from Guyana to southern Brazil (McConnell, 1968; Harmann et al., 1998; Gallagher & Brown, 1999), suggests that continental weathering could have played a role in the late Cretaceous pCO_2 decrease and climate cooling.

Over the last decades, the potential role of orogenesis on climate has been repeatedly pointed out, as mountain uplift typically promotes mechanical erosion and high chemical dissolution rates (Raymo et al., 1988; West et al., 2005; Gabet & Mudd, 2009). During the late Cretaceous, a major exhumation phase of the southeast American margin occurred (Gallagher & Brown, 1999; Franco-Magalhaes et al., 2010; Engelmann de Oliveira et al., 2016). This major tectonic event was subsequently followed by intense erosional processes, as inferred from apatite fission track data, which suggest erosion of up to 3 km of crust in Brazil (Gallagher & Brown, 1999; Engelmann de Oliveira et al., 2016) and the accumulation of thick sediment deposits on adjacent continental margins (Modica & Brush, 2004; Engelmann de Oliveira et al., 2016). Extensive mountain building at that time was most likely associated with enhanced continental chemical weathering of uplifted rocks, which could have driven active CO_2 consumption contributing to the late Cretaceous cooling. Yet this hypothesis has never been investigated so far.

Several isotopic proxies have been used to reconstruct the long-term evolution of silicate weathering, such as Sr, Os, Ca, or Li isotopes, using both carbonate record of ancient seawater chemistry and detrital sediments (Raymo et al., 1988; Derry & France-Lanord, 1996; Peucker-Ehrenbrinck & Ravizza, 2000). While providing interesting constraints on past weathering conditions, these proxies are also crucially dependent of additional processes, such as post-depositional alteration or various source effects, which complicate their use to track past changes in continental weathering (Raymo et al., 1988; Derry & France-Lanord, 1996).

In addition, the residence time of these elements in seawater is much higher that the oceanic mixing time, meaning that they display a homogeneous isotopic composition in the ocean, thereby preventing one to determine the region experiencing major chemical weathering changes at that time. Identifying the specific areas subject to major chemical weathering changes is however crucial for our understanding of the climate-tectonic links as it allows to explore the response of continental weathering to particular tectonic events occurring within different climatic belts.

In this study, we explored the potential links between tectonics, weathering and climate during the late Cretaceous using a new proxy for continental silicate weathering based on coupled measurements of hafnium and neodymium radiogenic isotopes in the clay-size fractions of fine-grained detrital sediments (Bayon et al., 2016). This new approach, complemented by clay mineral and elemental analyses, was applied here to sediments recovered from DSDP Site 356 offshore the Brazilian margin, with the aim to reconstruct the response of continental chemical weathering to the late Cretaceous uplift of the South American margin.

2. Setting

The southeastern Brazilian margin (Fig.1.A; Fig.1.B) is composed of the offshore Campos, Santos and Pelotas sedimentary basins, in addition to a narrow coastal plain that is bordered by the high-elevation regions of the Serra do Mar and the Serra da Mantiquera (Engelmann de Oliveira et al., 2016; Fig. 1.B). The studied DSDP site 356 is located on the southeast border of the São Paulo Plateau, close to the Santos Basin (Perch-Nielsen et al., 1977; Kumar et al., 1979; Fig. 1.B). During the late Cretaceous, Site 356 is thought to have been located within an arid climatic zone at 30°S (Basilici et al., 2009; Hay et al., 2012 Fig. 1.A). Studied samples were collected in fine sediments (mudstone or marly chalk) along three lithostratigraphical

units (Fig.2; Supplementary Table 1): (1) the Turonian/Coniacian, composed of clay-pebble conglomerate interbedded with mudstones, (2) the Santonian to mid-Maastrichtian, composed of marly-calcareous chalks and (3) the end of the Maastrichtian characterized by nannofossil- and foraminifer-rich marly-chalk. These sediments were deposited on an offshore margin at a paleodepth estimated at about 1000m or less (Perch-Nielsen et al., 1977), under direct influence of terrigenous inputs from the adjacent continental margin (Gallagher & Brown, 1999; Kumar & Gambôa, 1979).

The sediment source regions include an 1) Archean basement mostly exposed north of Site 356 (São Francisco Craton) and in the Luis Alves Craton, both mainly composed of granitoids, 2) Neoproterozoic basement composing the main part of the coast and 3) various Phanerozoic siliciclastic and carbonaceous rocks from the inland Paraná Basin and the Paraná-Etendeka basaltic province (~130 Ma) (Franco-Magalhaes et al., 2010; Engelmann de Oliveira et al., 2016; Fig. 1.B; Supplementary Table 2). Metasedimentary and metavolcanic rocks, composed among others of granitoids, orthogneisses, metapelites or migmatites, form the units from the Archean to the Cambrian (Franco-Magalhaes et al., 2010; Engelmann de Oliveira et al., 2016; the detailed lithology is provided in Supplementary Table 2).

3. Material and Methods

A total of 142 samples from Site 356 were analysed, spanning a period from the late Turonian (93.26 Ma) to the early Paleogene (65.98 Ma). The age model is based on Kochhann et al. (2014) and Gradstein et al. (2012).

3.1. Mineralogical analyses

X-ray diffraction (XRD) measurements for bulk sediment and clay (<2µm) mineralogy were performed using a Bruker Endeavor D4 diffractometer equipped with a Lynxeye detector, CuKα radiations and Ni filter, under 40 kV voltage and 25 mA intensity, at the Biogeosciences Laboratory (University of Burgundy, France).

The clay fraction was isolated and XRD analyses performed using three treatments as recommended by Moore & Reynolds (1997). Mineral phases were identified and quantified with the software MacDiff 4.2.5 using respectively the position of mean diffraction peaks and area of their main diffraction peak. Estimated proportions of clay mineral were performed on ethylene glycol solvated preparations using their main diffraction (d_{001}) peak. The palygorskite/illite ratio (P/I) and the (illite+chlorite)/smectite ratio ((I+C)/S) are calculated using the main diffraction peak area of each mineral. Replicate analyses of samples and the internal procedure of quantification using MacDiff on mixtures of clay minerals in known proportions allow to estimate the uncertainty of the relative proportions of the clay minerals as 5%.

The clay fraction <2µm of 4 samples was dispersed in distilled water and butylamine solution and then deposited on a carbon formvar Cu grid for Transmission electron microscopy (TEM) observations. Images of clay particles were performed using a JEOL JEM 2100F at the ARCEN analysis centre of the Université de Bourgogne equipped with a Bruker XFlash Detector 5030 spectrometer for EDX chemical analyses.

3.2. Geochemical analyses

3.2.1. Hf-Nd isotopes

A total of 21 samples (4 mudstone samples from Turonian/Coniacian and 17 marly - chalk samples from Coniacian to Maastrichtian) were selected for geochemical analyses. After grinding, about 1.5 g of bulk samples were treated with a sequential leaching procedure

that successively remove carbonates (with 10% v/v acetic acid (AA); overnight), Fe-Mn oxyhydroxide phases (with 0.05 M hydroxylamine hydrochloride solution (HH) in 15 % AA; 6 h) and organic matter (with 5% H_2O_2; overnight), derived from Bayon et al. (2002). The clay fraction (<2µm) was then isolate after decantation of the suspension during 95 min following Stokes law. A second round of sequential leaching was further applied to isolated clay fractions, in order to achieve quantitative removal of both Fe-Mn oxy-hydroxides and organic matter.

Clay-size samples and 5 certified reference materials from the United States Geological Survey (BCR-1, BCR-2, BIR-1, MAG-1, BHVO-2) were digested by alkaline fusion following the protocol of Bayon et al. (2009b). About 75 mg of dried powered clays were placed into a glassy carbon crucible, together with a Tm spike (a known weight around 50 ng which is used as an internal standard for the trace elements quantification according to the method developed by Barrat et al., 1996) and digested with Na_2O_2 (1.2 g) and NaOH (0.6 g) within a muffle furnace at 650°C for 12 min. Subsequent addition of ultrapure water to the resulting melt resulted in co-precipitation of Fe hydroxides. After centrifugation, all co-precipitated Fe hydroxides (containing reactive trace elements such as rare earth elements and hafnium) were dissolved with 5 ml HCl 4M and stored for subsequent analyses (i.e. called mother solutions thereafter).

Trace element concentrations (i.e. REE, Hf and Zr) were determined in samples by inductively coupled plasma mass spectrometry (ICP-MS) on a Thermo Scientific X-Series II at the Pole Spectrométrie Ocean (Brest, France). Measurements were performed on 2% HNO_3 solutions prepared from an aliquot of the mother solutions with a total dilution factor of about 3000, following the procedure of Barrat et al. (1996). Details about measured elemental masses, poly-atomic interference corrections and the quantification method are available in Freslon et al. (2011). External reproducibility and accuracy were estimated by analysing 2 to 4

replicates of 5 certified reference materials from the United States Geological Survey (BCR-1, BCR-2, BIR-1, MAG-1, BHVO-2), presented in supplementary material Table 3. Analytical reproducibility was better than 3% for all elements. Deviations to the reference values for BHVO-2, BCR-1, BCR-2 and BIR-1 (Jochum et al., 2016) were always < 6% RSD.

Purified hafnium and neodymium fractions were isolated from mother solutions by conventional ion chromatography using columns packed with AG-1X-8 resin for Hf and AG-50-X8 resin for Nd to isolate REE, then using Ln spec resin for both Hf and Nd, following the protocol described in Chu et al. (2002) and Bayon et al. (2012). Hafnium and neodymium isotopic measurements were performed on a MC-ICP-MS Neptune Plus (Thermo Scientific) at the ENS of Lyon (France), using a sample-standard bracketing method. The instrumental mass bias were corrected with the exponential law, using $^{146}Nd/^{144}Nd = 0.7219$ and $^{179}Hf/^{177}Hf = 0.7325$. Nd and Hf procedural blanks were respectively better than 22 pg and 25 pg.

Hf isotopic compositions were determined using a sample-standard bracketing method, analysing JMC 475 standard solutions having similar concentration than analysed samples. Mass-bias corrected values for $^{176}Hf/^{177}Hf$ were normalized to a JMC 475 value of 0.282163 (Blichert-Toft et al., 1997). Repeated analyses of bracketed JMC 475 standard during the analytical session gave a $^{176}Hf/^{177}Hf$ ratio of 0.282163 ± 0.000007 (2 s.d., n=17, 30ppb solution), corresponding to an external reproducibility of ± 0.25ε (2 s.d.). The overall analytical reproducibility and accuracy of the method was estimated by 3 replicates of the BHVO-2 reference material, which gave a $^{176}Hf/^{177}Hf$ value of 0.283099 ± 0.000005 (2 s.d., n=3), in agreement with the reference values of 0.283096 ± 0.000020 (Weis et al., 2005). The data are expressed with the standard epsilon notation $\varepsilon_{Hf}(t) = [((^{176}Hf/^{177}Hf)_{sample}/(^{176}Hf/^{177}Hf)_{CHUR}) - 1] * 10^4)$, corrected for the radioactive decay of ^{176}Lu to ^{177}Hf using the Hf and Lu concentrations measured for each sample ($^{176}Lu/^{177}Hf = Lu/Hf *$

0.1424), the absolute age (t) calculated for each sample based on the age model of Kochhann et al. (2014) and the timescale of Gradstein et al. (2012), and the ^{176}Lu radioactive decay constant λ (1.867×10^{-11} an^{-1}; Söderlund et al., 2004). The CHUR (CHondritic Uniform Reservoir) ^{176}Hf/^{177}Hf ratio was corrected using a present-day value of 0.282785 and a ^{176}Lu/^{177}Hf ratio of 0.0336 (Bouvier et al., 2008).

Nd isotopic compositions were determined by analysing JNdi-1 standard solutions with comparable concentrations every two or three samples. Mass-bias corrected values for ^{143}Nd/^{144}Nd were normalized to a JNdi-1 value of 0.512115 (Tanaka et al., 2000) using a sample-standard bracketing method. Analyses of the bracketed JNdi-1 standard during the analytical session gave a ^{143}Nd/^{144}Nd ratio of 0.512115 ± 0.000012 (2 s.d., n=18, 50ppb solution), corresponding to an external reproductibility of ± 0.23ε (2 s.d.). Analyses of BHVO-2 and BCR-2 reference materials gave a ^{143}Nd/^{144}Nd value of 0.512986 ± 0.000005 (2 s.d., n=3), close to the published values of 0.512990 ± 0.000010 (Weis et al., 2006), and of 0.512634 ± 0.000005 (2 s.d., n=3), close to the published values of 0.512638 ± 0.000015 (Weis et al., 2006), respectively. The data are reported in the standard epsilon notation $\varepsilon_{Nd} = [((^{143}Nd/^{144}Nd)_{sample}/(^{143}Nd/^{144}Nd)_{CHUR}) - 1] * 10^4)$, corrected for the radioactive decay of ^{147}Sm to ^{143}Nd based on the Nd and Sm concentrations measured for each sample (^{147}Sm/^{144}Nd = Sm/Nd * 0.6049), the absolute age (t) calculated for each sample and the ^{147}Sm radioactive decay constant λ (6.54×10^{-12} an^{-1}; Lugmair & Marti, 1977). The CHUR (CHondritic Uniform Reservoir) ^{143}Nd/^{144}Nd ratio were also corrected using a present-day value of 0.512630 and a ^{147}Sm/^{144}Nd ratio of 0.1960 (Bouvier et al., 2008).

3.2.2. Major elements concentrations analyses and CIA

Whole-rock major element abundances (SiO_2, TiO_2, Al_2O_3, Fe_2O_3, MnO, MgO, CaO, Na_2O, K_2O, Cr_2O_3, P_2O_5 and NiO) were determined by X-ray fluorescence (XRF) at the University

of Lausanne, using a wavelength-dispersive PANalytical Axios^{mAX} spectrometer fitted with a 4 kW Rh X-ray tube. The analyses were performed on fused disks prepared from 1.2 g of calcined sample powder mixed with Lithium-Tetraborat (1:5 mixture). The XRF calibrations are based on 21 international silicate rock reference materials. The data are reported on a loss of ignition (*LOI*)-free basis (Supplementary Table 1). The limits of detection depend on the element concerned but are in the range 20 to 80 ppm for major elements.

The CIA ($Al_2O_3/[Al_2O_3 + Na_2O + CaO^* + K_20] * 100$, where CaO* represents the amount of CaO in the silicate fraction of the sediments is used as a proxy of chemical weathering intensity and is generally interpreted as the extent to which feldspar, which contains relatively mobile Ca, Na and K, has been transformed into Al-rich clay minerals (Nesbitt & Young, 1982).

Because our sample are carbonate-rich (in the 29-62 % range, except for one samples (40r2w110) that yield 0.35 %), detrital CaO contents were estimated using the method of McLennan (1993), which consists in replacing CaO* by Na_2O.

4. Results and Discussion

4.1. Tectonic pulse during the Turonian to Santonian favouring enhanced mechanical erosion

The large tectonic uplift that affected the eastern South American margin during the late Cretaceous, and gave birth to the Serra do Mar and the Serra da Mantiquera, occurred during the 92 to 70 Ma time interval (Gallagher & Brown, 1999; Franco-Magalhaes et al., 2010; Engelmann de Oliveira et al., 2016). Following uplift, enhanced mechanical erosion typically results in the export of coarser siliciclastic material (feldspar, micas and quartz), primary clay

minerals (e.g. illite, chlorite, cf. Chamley 1989) and heavy accessory minerals (e.g. ilmenite, rutile) that influence bulk sediment geochemical signatures, such as the Ti/Al ratio. Heavy accessory minerals tend to be enriched in Ti, and the Ti/Al ratio is thus classically used as an indicator of enhanced physical erosion, reflecting the increasing contribution of coarse-grained detrital particles in the sediment deposited at margins (e.g. Zabel et al., 1999; Chen et al., 2013; Fantasia et al., 2019; Fig. 3). Therefore, these mineralogical and geochemical proxies can be used here to help refining the timing of the tectonic pulse affecting the southeastern Brazilian margin. Illite (I) and chlorite (C) are considered as primary clay minerals resulting from mechanical erosion of igneous and old sedimentary rocks, associated to limited chemical weathering, such as what is commonly observed under dry climate conditions and/or in active tectonic settings where minerals are removed too fast from source rock regions (Chamley, 1989). By contrast, smectites (S) are formed in soils by more intense chemical weathering of silicate minerals (bisiallitisation), under semi-arid or temperate-humid climate (Chamley, 1989; Ruffel et al., 2002). Thus, a tectonic uplift episode is expected to result in an increase in the proportion of primary clay minerals in the clay assemblages transported and deposited offshore, reflected by high (I+C)/S ratio (Fig. 3). To a first approximation, this ratio can thus be used to infer the intensity of erosion following uplift.

In agreement with previous study (Robert, 1981; Zimmerman et al., 1977), the clay mineral assemblage at Site 356 is mainly composed of smectite (76 to 95% of the assemblage), followed by illite (up to 15%), palygorskite (up to 8%), and traces of chlorite and kaolinite (Fig. 2; Supplementary Table 1). The overabundance of smectite is a common feature of upper Cretaceous marine sediments, which was shown to be mainly of terrigenous origin (Robert, 1981; Chamley, 1989). The detrital origin of smectites at Site 356 is further supported by their morphology as observed with TEM displaying a flaky shape characteristic of detrital particles (Fig. 4), in contrast to authigenic smectite, which typically exhibits lath-

shape overgrowths (Clauer et al., 1990). Palygorskite also displays features typical of a detrital origin, as inferred from short and broken fibres (Fig. 4), which attest that clay minerals in the sediment are mostly inherited from nearby continental landmasses. The rare earth element (REE) composition of the clay-size fraction of sediments additionally point towards a detrital origin for the clays, since no enrichment of heavy rare earth elements (HREE) nor negative cerium anomaly were observed (Fig. 5), as it would have been otherwise expected in the presence of authigenic clays (Fagel 1992; Bayon et al., 2015). As already pointed out by Zimmerman (1977) and Robert (1981), late diagenesis at Site 356 is unlikely to have affected clay mineral assemblages, as inferred from the presence of clay minerals that are sensitive to burial diagenesis, such as smectite and palygorskite. Therefore, we interpret hereafter the (I+C)/S ratio as reflecting the importance of mechanical erosion processes relative to chemical weathering processes affecting the adjacent margin.

Despite limited downcore variation in the proportion of illite and chlorite relative to smectite, the (I+C)/S ratio decreases significantly between the Santonian and Middle Campanian (Fig. 3). The observed decrease in the proportion of primary clay minerals during this interval likely results from a decrease of mechanical erosion and/or an increase in chemical weathering intensity.

A decrease in mechanical erosion is further supported by the bulk sediment Ti/Al ratio, which similarly decreases during the Santonian to Middle Campanian time interval, together with the observed depletion in quartz (Q) and K-feldspar (FK) relative to clays in the bulk sediment (Fig. 3; Supplementary Fig. S1, Fig. S2), hence also suggesting lower denudation rates. In contrast, higher denudation rates during the earlier Turonian to Santonian are supported both by higher (I+C)/S and (Q+FK)/Clay values (Supplementary Fig. S1, Fig. S2) and higher bulk sediment Ti/Al values. Altogether, the above mineralogical and geochemical evidence thus suggest that enhanced mechanical erosion prevailed during the Turonian to the Santonian

interval, associated with enhanced detrital inputs being delivered to the nearby southeastern Brazilian margin. Linking enhanced erosion to the uplift of the southeastern Brazilian margin, our new data would then highlight a tectonic pulse of the margin during the Turonian to the Santonian (92 Ma to around 84 Ma), thus refining the overall interval suggested by AFTA data (Gallagher & Brown, 1999; Franco-Magalhaes et al., 2010; Engelmann de Oliveira et al., 2016).

4.2. A change in the source of sediment associated to the southeastern Brazilian margin uplift

Following this tectonic pulse, a change in the geographic provenance of the sediment deposited at Site 356 is shown by a decrease in clay $\varepsilon_{Nd(t)}$ during the Santonian and Campanian, from values of about -8 ε-units during the Turonian-Coniacian to more unradiogenic values of about -11 ε-units in the Maastrichtian (Fig. 2; Fig.3). Although the contribution of volcanogenic material may be overestimated in the clay-size fraction of river-borne sediments (Garçon and Chauvel, 2014; Bayon et al., 2015), the fine-grained detrital material eroded transported by rivers is generally assumed to provide a reliable estimate of the Nd isotope composition of the exposed source rocks in corresponding catchments (Frank, 2002; Goldstein et al., 2003). The Nd isotopic composition of detrital sediments has thus be widely used as a tracer of sediment provenance (e.g. Frank, 2002).

Based on seismic stratigraphy in the São Paulo Plateau and Santos Basin, Kumar & Gambôa, (1979) showed that the sediments deposited at Site 356 come from the erosion of the adjacent southeastern Brazilian margin. We have completed the compilation of $\varepsilon_{Nd(t)}$ data initiated by Mantovanelli et al. (2018) of the Brazilian margin (Supplementary Table 2; Fig. 1.B). The compilation reveals that the southeastern Brazilian margin encompasses a wide range of Nd isotope compositions that defines three potential source end-members represented on Figure 1

(Fig. 1.B; Mantovanelli et al., 2018; Supplementary Table 2). The first group corresponds to the most radiogenic (high ε_{Nd}) values, ranging between -10.4 to +3.3 ε-units, and is composed of the Paraná Basin (Fig. 1.B), the Paraná-Etendeka basaltic province, the Rio Negro Magmatic Arc and some other Proterozoic formations with juvenile source material (e.g. Neoproterozoic juvenile Cambai magmatic arc complex; Supplementary Table 2). The second group yields values ranging between -18.0 and -12.7 ε-units and corresponds to the Mesoproterozoic-Neoproterozoic basement (Fig. 1.B). Finally, the third group shows quite unradiogenic values ranging from -34.9 to -18.0 ε-units associated with the Archean-Paleoproterozoic cratons (São Francisco Craton, Luis Alves Craton, Fig. 1.B) and other Proterozoic formations with older magmatic sources, particularly in the Ponta Grossa Arch (Fig. 1.B).

The clay fraction at Site 356 reflects a mixture of these different sources, with a more pronounced contribution of the quite radiogenic Paraná Basin and Paraná-Etendeka basaltic province during the Turonian to Coniacian interval. The observed decrease in $\varepsilon_{Nd(t)}$ values down to -11.2 ε-units during the Santonian to Maastrichtian highlights a change in sediment provenance, associated with decreasing contribution of the above mentioned radiogenic sedimentary sources to the sediment deposited at the studied site. This change in the source of the sediment deposited at Site 356 could have also partly contributed to the observed Ti/Al decrease starting from the Santonian. Indeed, variations in bulk sediment Ti/Al ratio could be partly driven by changes in the relative contribution of mafic/felsic rock sources. This is because Ti is typically more concentrated in mafic/volcanic rocks (Rudnick and Fountain, 1995), hence leading to higher Ti/Al ratios in sediments resulting from the erosion of mafic rocks (Chen et al., 2011). Thus, the observed decrease in the relative contribution of mafic detrital material from the Santonian onward, as inferred from the shift towards lower $\varepsilon_{Nd(t)}$ values, may have also contributed to the decrease in Ti/Al ratio from the Santonian.

Most likely, the observed shift in sediment provenance after the Coniacian was driven by the tectonic reorganization that affected the southeastern Brazilian margin during the Turonian to Santonian. This uplift was associated with a westward tilt of the margin, which probably modified the drainage pattern and, as a consequence, resulted in reduced export of the sediment load from the Paraná-Etendeka inland province. Changes in the drainage pattern is further supported by evidence for the development of the Paraíba do Sul River that drained the Neoproterozoic basement during the late Cretaceous, which could also have resulted in a greater contribution of unradiogenic terrigenous material to the adjacent oceanic basins (Engelmann de Oliveira et al., 2016; Modica & Brush, 2004). Additionally, the tectonic reorganization could have favored the development of floodplains in the foreland area of the freshly exposed mountain range, which could have promoted more intense chemical weathering and formation of secondary minerals such as smectites (Bouchez et al., 2012).

4.3. Using Hf-Nd isotopes in clays to trace silicate weathering intensity

Enhanced mechanical erosion is considered to promote chemical weathering as it leads to exposure of fresh rock surfaces (Raymo et al., 1988; West et al., 2005; Gabet & Mudd, 2009). Yet, in active tectonic settings characterized by high denudation rates, the rate of export of detrital material can be more rapid than silicate mineral dissolution, leading to chemical weathering rates that remain constant or may even decrease with increasing denudation rates (White & Blum, 1995; Gabet & Mudd, 2009, West, 2012). Additionally, climatic parameters such as temperature and precipitation also play a major role in controlling chemical weathering rates (Brady, 1991; White & Blum, 1995).

Recent studies in modern environments have shown that the combined Lu-Hf and Sm-Nd isotope systems in clays can be used to track changes in continental chemical weathering (Bayon et al., 2009a, 2016). Both Lu-Hf and Sm-Nd isotopic systems behave similarly during

magmatic processes, resulting in terrestrial rocks that display a broad correlation in a ε_{Nd} - ε_{Hf} plot ("terrestrial array" on Fig. 6; Vervoort et al., 1999), where mantle-derived rocks are characterized by radiogenic (high) ε_{Nd} and ε_{Hf} composition, while old crustal material displays unradiogenic (low) ε_{Nd} and ε_{Hf} values. However, the Lu-Hf and Sm-Nd isotope systems are decoupled during weathering processes. A large part of the ε_{Nd} and ε_{Hf} decoupling during surface processes arises from mineral sorting during sediment transport and deposition (Vervoort et al., 1999; Chauvel et al., 2014), which result in preferential enrichment of zircons into coarse-grained sediment fractions. Zircons dominate the Hf budget in terrestrial rocks and sediments, being typically characterized by very low ε_{Hf} (unradiogenic) compositions. By contrast, the Hf isotopic composition of the fine-grained zircon-poor clay-size fractions of sediment is generally characterized by more radiogenic ε_{Hf} values plotting above the Terrestrial Array. The correlation displayed by clay ε_{Nd} and ε_{Hf} in a ε_{Nd} - ε_{Hf} plot, the so-called "Clay Array" (Fig. 6; Bayon et al., 2016) is thus distinct from the Terrestrial Array.

As a consequence, any 'vertical' departure of clay ε_{Hf} from the Clay Array in the ε_{Nd} - ε_{Hf} plot ($\Delta\varepsilon_{Hf(t)clay}$; Fig. 6) can be interpreted as reflecting the relative contribution of unweathered primary detrital minerals with low ε_{Hf} values and of secondary clay minerals with high ε_{Hf}. Indeed, whereas weathering products generally display similar Nd isotope composition, Lu-rich mineral phases are preferentially dissolved during chemical weathering (Bayon et al., 2006; Dausmann et al., 2019), leading to significant release of dissolved radiogenic Hf fraction that can be subsequently incorporated in the secondary clay minerals formed in soils (Bayon et al., 2016). Enhanced silicate chemical weathering both promotes the release of radiogenic Hf in solution and increases the relative contribution of radiogenic secondary clays in the < 2µm fraction of sediments relative to fine-grained primary minerals with less radiogenic Hf isotopic composition, which both results in an increase of $\Delta\varepsilon_{Hf(t)clay}$. Thus within the zircon-depleted clay-size fraction of river sediments, it has been shown that

$\Delta\varepsilon_{Hf(t)clay}$ provides information on chemical weathering intensity in corresponding source regions (Bayon et al., 2016). Zr concentrations in our analysed <2µm fractions (184 ppm on average and not higher than 258 ppm) are within the range of modern zircon-poor clay-size fractions (Bayon et al., 2016). Importantly, no significant correlation is observed in our data between $\varepsilon_{Hf(t)}$ values and Zr concentrations (Fig. 7), nor between $\Delta\varepsilon_{Hf(t)clay}$ and Zr concentrations, hence implying that the evolution of ε_{Hf} and $\Delta\varepsilon_{Hf(t)clay}$ in our sediment record is unlikely to be driven by the presence of zircons in the analysed clay fractions.

Measured $\Delta\varepsilon_{Hf(t)clay}$ values increase during the Santonian and Campanian, from ~-3.0 ε-units in the Turonian and Coniacian to about 1.7 ε-units in the Maastrichtian (Fig. 2; Fig.3). A strong correlation can be noted between $\Delta\varepsilon_{Hf(t)clay}$ and $\varepsilon_{Nd(t)}$ (Fig.7), which could possibly indicate a link between $\Delta\varepsilon_{Hf(t)clay}$ and the source of the eroded sediments. Presumably, the alteration of old crustal material could release more radiogenic Hf than weathering of younger crustal material due to increasing ε_{Hf} differences between rock-forming minerals with time. This effect certainly explains the increasing offset of clay $\varepsilon_{Hf(t)}$ from the Terrestrial Array with increasing age of the source crustal rock (i.e. with lower ε_{Nd} values) (Fig.6). However, $\Delta\varepsilon_{Hf(t)clay}$ represents the departure of $\varepsilon_{Hf(t)}$ from the Clay Array and the distribution of $\Delta\varepsilon_{Hf(t)clay}$ in modern world river clays does not appear to be controlled by the age of corresponding source rocks, but instead by environmental parameters and chemical weathering intensity (Bayon et al., 2016). Thus, although a possible source control on $\Delta\varepsilon_{Hf(t)clay}$ cannot be entirely excluded at this point, we are confident that the observed $\Delta\varepsilon_{Hf(t)clay}$ variability at Site 356 is not primarily driven by the mean age of corresponding source rocks. This is further supported by the fact that $\Delta\varepsilon_{Hf(t)clay}$ does not correlate with the sediment lithology at Site 356 (Fig.2, Supplementary Table 1).

Most likely, the apparent relationship between $\Delta\varepsilon_{Hf(t)clay}$ and $\varepsilon_{Nd(t)}$ indicates that the uplift of the southeastern Brazilian margin was accompanied by a progressive change in the source of

the sediment exposed to erosion, leading to a shift of $\varepsilon_{Nd(t)}$ from the Santonian (Fig.2; Fig. 3), due possibly to a westward tilt of the margin and reorganization of the the drainage pattern; but also, simultaneously, leading to locally more intense hydrolyzing conditions, which resulted in more intense chemical weathering and thus higher $\Delta\varepsilon_{Hf(t)clay}$.

4.4. An increase in local hydrolysis conditions suggested by clay mineral assemblages

A change in hydrolysis conditions, initiating during the Turonian and accelerating during the Campanian, is also supported by the evolution of clay mineralogical assemblages. Clay minerals have been used by many authors for paleoenvironmental reconstructions and can provide some insights on the evolution of humidity/aridity conditions on the South American eastern margin (e.g. Chamley, 1989; Ruffel et al., 2002; Dera et al., 2009 ; Chenot et al., 2018 ; Fantasia et al., 2019). At Site 356, the presence of smectite-rich clay mineral assemblages is consistent with a warm, semi-arid and seasonal climate, which would have resulted in the formation of smectite in soils from the nearby continent. The clay assemblages are also marked by higher proportions (up to 8 %) of palygorskite from the Turonian to Santonian, although the proportions are probably underestimated here due to the diffraction pattern of such fibrous magnesium clays (e.g. Pletsch, 2001; Ouhadi et al., 2003; Fig. 2, Fig. 4). Palygorskite precipitates principally in evaporative basins, such as in inland seas, lakes and other peri-marine environments under sub-arid or seasonally arid conditions (Callen, 1984; Chamley, 1989). Some cases of authigenic precipitation of fibrous clays in the marine environment are however well known in Upper Cretaceous sediments (Callen, 1984; Daoudi, 2004). Yet as described in section 4.1, TEM observation shows short and broken palygorskite fibres, clearly attesting of the detrital origin of this mineral at Site 356.

The evolution of clay mineralogy at Site 356 shows a marked decrease of the palygorskite/illite ratio (P/I; Fig. 3), which we interpret here as reflecting a shift from arid to more hydrolysing conditions throughout the Turonian to Maastrichtian interval, with an acceleration during the Campanian. This evolution is consistent with the increase in smectite proportions in the clay assemblages and the decrease of the (I+C)/S ratio (Fig. 2, Fig. 3). To some extent, a change in the source of sediments could also potentially drive changes in clay mineral assemblages. Yet at this site, the observed increase in smectite proportions cannot result from a change in the source of sediments, which would require an increasing proportion of mafic rock source erosion and weathering (Chamley 1989; Ruffel et al., 2002) that is not supported by the evolution of $\varepsilon_{Nd(t)}$ during this interval. Higher proportions of smectite after the Santonian is thus better explained by more hydrolysing conditions, also consistent with the decrease of palygorskite contents (Fig.2; Fig.3). A climatic evolution towards more humid conditions is additionally supported by the progressive apparition of kaolinite, though in small proportions, during the Maastrichtian (Robert & Chamley, 1987; Fig. 2). Kaolinite is a clay mineral commonly associated to intense chemical weathering under hot and wet climate with optimal drainage conditions (Chamley, 1989; Thiry, 2000; Ruffel et al., 2002). This change in clay mineralogical assemblages, that is most pronounced after the Santonian, occurred at the end of the uplift pulse of the nearby Brazilian margin as depicted by the high (I+C)/S and Ti/Al evolution in the Turonian to Santonian interval (Fig. 3).

Interestingly, a strong correlation can also be observed between clay $\varepsilon_{Nd(t)}$ values and smectite and palygorskite proportions (Fig. 7). As detrital fraction $\varepsilon_{Nd(t)}$ is not impacted by changes in hydrolysing conditions, the negative correlation with smectite proportions and positive correlation with palygorskite proportions may only result from a temporal coincidence between change in the source of sediments impacting $\varepsilon_{Nd(t)}$ but not clay assemblages and a change in hydrolysing conditions favouring smectite formation. By contrast the positive

correlation displayed by $\Delta\varepsilon_{Hf(t)clay}$ and smectite contents and its negative correlation with palygorskite contents in clays (Fig. 7) highlight the dependence of $\Delta\varepsilon_{Hf(t)clay}$ to hydrolysing conditions, coherent with the strong relationships observed between $\Delta\varepsilon_{Hf(t)clay}$ and mean annual precipitations in modern environments (Bayon et al., 2016).

The apparent co-evolution of sediment provenance and local hydrolysis / chemical weathering intensity hence supports the view that the correlation between $\Delta\varepsilon_{Hf(t)clay}$ and $\varepsilon_{Nd(t)}$ is most likely coincidental. We therefore interpret hereafter the observed increase in $\Delta\varepsilon_{Hf(t)clay}$ values during the Santonian and Campanian as reflecting an intensification of chemical weathering on the nearby continent.

4.5. Enhanced weathering and tectonic uplift : a rain shadow effect?

The Chemical Index of Alteration (CIA) determined from major element concentrations provides additional support for an evolution of chemical weathering during the studied interval. The CIA measures the degree of mobile element depletion relative to immobile elements during chemical weathering (Nesbitt & Young, 1982). This index is however also controlled by sediment source and mineralogical sorting during sediment transport (Fantasia et al., 2019), which impedes its application to various geological settings. At Site 356, $\varepsilon_{Nd(t)}$ values indicate a change in the source of sediments, with a larger contribution of mafic rocks from the Parana-Etendeka Province during the Turonian to Coniacian, that decreases from the Santonian onward. This change in sediment provenance would be expected to decrease CIA values, as Na and K, used here in our CIA calculation (see methodology section), are usually more abundant in crustal material than in mantellic material. An increasing proportion of old crustal material at Site 356 through time, as inferred from decreasing ε_{Nd} values, should have been accompanied by lower CIA values, hence opposite to what is observed here (Fig. 3). As

a consequence, the CIA evolution observed at Site 356, although being moderate, provides additional support in favor of an increase in chemical weathering intensity from the Santonian to Maastrichtian. Based on the new overall dataset, combining clay mineralogical assemblages, Ti/Al, CIA and $\Delta\varepsilon_{Hf(t)clay}$, we thus propose here that the tectonic pulse would have occurred in a relatively arid climate that would have limited chemical weathering despite potentially high erosion rates. The onset of the relief parallel to the coast could have promoted the establishment of a locally more hydrolysing climate on the eastern side of the relief, evidenced by increasing proportions of smectites and decreasing proportions of palygorskite, and thus enhanced chemical weathering as depicted by $\Delta\varepsilon_{Hf(t)clay}$, supported by CIA, from the Santonian onward. Indeed, the formation of a relief could favour condensation of the clouds formed in the nearby ocean as the air becomes cooler with altitude (rain shadow effect). This tectonic uplift event has already been linked to a change in local climate by Garcia et al. (2005), Basilici et al. (2009) and Fernandes & Magalhães (2015) in their studies of the Bauru Basin. These authors interpreted the increasing aridity observed during the late Cretaceous in the Bauru Basin, located inland, as a consequence of a rain shadow effect with clouds blocked eastward by the forming relief. If such an effect could have increased aridity inland, it would have promoted a more humid climate and subsequent chemical weathering on the eastern flank of the newly created relief, or in active floodplains that may have progressively developed in the relief foreland area. The role of floodplains in chemical weathering of eroded material from tectonically active mountain belts has been repeatedly put forward, based on the long transfer time of sediments in these lowland areas (e.g. Bouchez et al., 2012; Bayon et al., 2020), in the modern Andes or Himalaya areas. This process could also have contributed to enhance chemical weathering of the erosional product from the Brazilian margin.

Importantly, our new data set indicate that the increase in chemical weathering intensity at the Brazilian margin during the Santonian and Campanian postdates the main uplift phase and

erosional event identified in the Turonian to Santonian. While tectonic uplift was most likely accompanied by higher denudation rates, the presence of thin soils and kinetically-limited weathering conditions would have presumably resulted in weak-to-moderate degrees of chemical weathering intensity during the uplift phase.

4.6. Uplift of the South-American margin: a driver for the late Cretaceous cooling?

Temperature also plays a major role in silicate weathering reactions (Brady, 1991; White & Blum, 1995). The late Cretaceous period experienced a major long-term climate cooling from the Turonian onward, with an acceleration from the Santonian to the middle Campanian that affected all latitudes (Friedrich et al., 2012; O'Brien et al., 2017; Fig. 3). In South America, this cooling period is documented in various sedimentary records from Demerara Rise, along the French Guiana margin, and at Site 511 on the Falkland Plateau (Huber et al., 1995; O'Brien et al., 2017), but no regional temperature record is available for the studied area.

Considering the positive relationship that exists between silicate weathering and temperature, the observed cooling that occurred from the Turonian onward would be expected to hamper silicate weathering. On the contrary, our $\Delta\varepsilon_{Hf(t)clay}$ data rather point to an increase in chemical weathering intensity of the Brazilian margin during the late Cretaceous, from the Santonian to the Maastrichtian that represents the coolest interval of the late Cretaceous. Thus, this increase in chemical weathering intensity appears unlikely to have been driven by the long-term climate evolution, but is better explained by regionally enhanced hydrolysing conditions promoted by relief formation and associated rain shadow effect.

Conversely, the coincidental occurrence of the increase in the intensity of chemical weathering in eastern South America inferred from our data at a time of global climate cooling suggests that the tectonic uplift of the eastern South American margin could have contributed to drive climate change during the late Cretaceous. Interestingly, the onset of

$\Delta\varepsilon_{Hf(t)clay}$ increase depicted from the Santonian onward coincides to or slightly predates the cooling acceleration recorded during the late Santonian to middle Campanian recorded at the global scale by benthic foraminifera $\delta^{18}O$ (Fig. 3). Insights on the role of mountain uplifts on global climate through silicate weathering and associated CO_2 drawdown largely rely on case studies taken from the late Cenozoic period and the uplift of the Himalayan-Tibetan Plateau (e.g. Raymo et al., 1988; Dupont-Nivet et al., 2008). While the role of uplift-driven silicate weathering on long-term climate change has been recently challenged (e.g. Willenbring & von Blanckenburg, 2010; Norton & Schlunegger, 2017), our new data re-emphasize the potential relevance of the uplift-climate hypothesis in the case of the late Cretaceous cooling and its possible link to the uplift of the southeastern South American margin. Although further studies would be required to validate this hypothesis and estimate the magnitude of the impact of silicate weathering on global climate change, our study represents an important step in the attempt to better understand the origin of the late Cretaceous climate cooling and its relationship to long-term changes in continental chemical weathering.

5. Conclusion

The combined Sm-Nd and Lu-Hf isotope systems, expressed by $\Delta\varepsilon_{Hf(t)clay}$, are successfully applied here for the first time to Cretaceous sediments to track variations in continental weathering intensity. In this work, both clay mineralogy and $\Delta\varepsilon_{Hf(t)clay}$ highlight a marked increase in chemical weathering of the nearby eastern South American margin from the Santonian to the Maastrichtian. This increase slightly postdates an episode of enhanced mechanical erosion likely linked to the uplift of the nearby Brazilian margin evidenced during the Turonian to Santonian interval by higher proportions of primary clay minerals (illite and chlorite), by higher Ti/Al values and by higher proportions of quartz and feldspar in the bulk

sediment. Uplift of the Brazilian margin would have led to the establishment of a locally more hydrolyzing climate on the eastern side of the formed relief (rain shadow effect), supported by decreasing palygorskite and increasing smectite proportions in sediments, enhancing chemical weathering of the margin. The development of floodplains in the foreland area of this relief could also have played a role in promoting efficient chemical weathering of erosional products favouring smectite formation. Importantly, the depicted increase in chemical weathering of the Brazilian margin is concomitant to a marked acceleration of the overall climate cooling recorded in the Campanian, highlighting for the first time a potentially important role of the eastern South American margin tectonic uplift in this climate decline. Our data thus provide new support to the uplift-climate hypothesis in deep time that still largely relies on the Himalayan-Tibetan uplift and Cenozoic cooling.

References

Barrat, J.A., Keller, F., Amossé, J., Taylor, R.N., Nesbitt, R.W., Hirata, T., 1996. Determination of Rare Earth Elements in Sixteen Silicate Reference Samples by Icp-Ms After Tm Addition and Ion Exchange Separation. Geostandards Newsletter 20, 133–139. https://doi.org/10.1111/j.1751-908X.1996.tb00177.x

Basilici, G., Bó, P.F.F.D., Ladeira, F.S.B., 2009. Climate-induced sediment-palaeosol cycles in a Late Cretaceous dry aeolian sand sheet: Marília Formation (North-West Bauru Basin, Brazil). Sedimentology 56, 1876–1904. https://doi.org/10.1111/j.1365-3091.2009.01061.x

Bayon, G., Burton, K.W., Soulet, G., Vigier, N., Dennielou, B., Etoubleau, J., Ponzevera, E., German, C.R., Nesbitt, R.W., 2009a. Hf and Nd isotopes in marine sediments: Constraints on global silicate weathering. Earth and Planetary Science Letters 277, 318–326. https://doi.org/10.1016/j.epsl.2008.10.028

Bayon, G., Barrat, J.A., Etoubleau, J., Benoit, M., Bollinger, C., Révillon, S., 2009b. Determination of Rare Earth Elements, Sc, Y, Zr, Ba, Hf and Th in Geological Samples by ICP-MS after Tm Addition and Alkaline Fusion. Geostandards and Geoanalytical Research 33, 51–62. https://doi.org/10.1111/j.1751-908X.2008.00880.x

Bayon, G., Dennielou, B., Etoubleau, J., Ponzevera, E., Toucanne, S., Bermell, S., 2012. Intensifying Weathering and Land Use in Iron Age Central Africa. Science 335, 1219–1222. https://doi.org/10.1126/science.1215400

Bayon, G., German, C.R., Boella, R.M., Milton, J.A., Taylor, R.N., Nesbitt, R.W., 2002. An improved method for extracting marine sediment fractions and its application to Sr and Nd isotopic analysis. Chemical Geology 187, 179–199. https://doi.org/10.1016/S0009-2541(01)00416-8

Bayon, G., Toucanne, S., Skonieczny, C., André, L., Bermell, S., Cheron, S., Dennielou, B., Etoubleau, J., Freslon, N., Gauchery, T., Germain, Y., Jorry, S.J., Ménot, G., Monin, L., Ponzevera, E., Rouget, M.-L., Tachikawa, K., Barrat, J.A., 2015. Rare earth elements and neodymium isotopes in world river sediments revisited. Geochimica et Cosmochimica Acta 170, 17–38. https://doi.org/10.1016/j.gca.2015.08.001

Bayon, G., Skonieczny, C., Delvigne, C., Toucanne, S., Bermell, S., Ponzevera, E., André, L., 2016. Environmental Hf–Nd isotopic decoupling in World river clays. Earth and Planetary Science Letters 438, 25–36. https://doi.org/10.1016/j.epsl.2016.01.010

Bayon, G., Vigier, N., Burton, K.W., Agnès Brenot, J.C., Etoubleau, J., Chu, N.-C., 2006. The control of weathering processes on riverine and seawater hafnium isotope ratios. Geology 34, 433–436. https://doi.org/10.1130/G22130.1

Bayon, G., Lambert, T., Vigier, N., De Deckker, P., Freslon, N., Jang, K., Larkin, C.S., Piotrowski, A.M., Tachikawa, K., Thollon, M., Tipper, E.T., 2020. Rare earth element and neodymium isotope tracing of sedimentary rock weathering. Chemical Geology

553, 119794. https://doi.org/10.1016/j.chemgeo.2020.119794

Berner, R. A., Lasaga, A. C., Garrels, R. M., 1983. The carbonate-silicate geochemical cycle and its effect on atmospheric carbon dioxide over the past 100 million years, Am. J. Sci. 283, 641-683.

Blichert-Toft, J., Chauvel, C., Albarède, F., 1997. Separation of Hf and Lu for high-precision isotope analysis of rock samples by magnetic sector-multiple collector ICP-MS. Contrib Mineral Petrol 127, 248–260. https://doi.org/10.1007/s004100050278

Bouchez, J., Gaillardet, J., Lupker, M., Louvat, P., France-Lanord, C., Maurice, L., Armijos, E., Moquet, J.-S., 2012. Floodplains of large rivers. Weathering reactors or simple silos? Chemical Geology 332–333, 166–184. https://doi.org/10.1016/j.chemgeo.2012.09.032

Bouvier, A., Vervoort, J.D., Patchett, P.J., 2003. The Lu–Hf and Sm–Nd isotopic composition of CHUR: Constraints from unequilibrated chondrites and implications for the bulk composition of terrestrial planets. Earth and Planetary Science Letters 273, 48–57. https://doi.org/10.1016/j.epsl.2008.06.010

Brady, P. V., 1991. The effect of silicate weathering on global temperature and atmospheric CO2. J. Geophysical Res. 96, 101–106.

Callen, R.A., 1984. Clays of the palygorskite-sepiolite group: Depositional environment, age and distribution. In Singer, A., Galan, E. (Eds.) Palygorskite-sepiolite occurrences, genesis and uses. Dev. Sedimentol. 37. Elsevier Sci. Publ. Co., Amsterdam, 1-37.

Chamley, H., 1989. Clay sedimentology ed. Springer-Verlag Berlin Heidelberg GmbH.

Chauvel, C., Garçon, M., Bureau, S., Besnault, A., Jahn, B., Ding, Z., 2014. Constraints from loess on the Hf–Nd isotopic composition of the upper continental crust. Earth and Planetary Science Letters 388, 48–58. https://doi.org/10.1016/j.epsl.2013.11.045

Chen, H.-F., Chang, Y.-P., Kao, S.-J., Chen, M.-T., Song, S.-R., Kuo, L.-W., Wen, S.-Y., Yang, T.-N., Lee, T.-Q. 2011. Mineralogical and geochemical investigations of sediment-source region changes in the Okinawa Trough during the past 100 ka (IMAGES core MD012404). Journal of Asian Earth Sciences 40 (6), 1238-1249.

Chen, H. F., Yeh, P. Y., Song, S. R., Hsu, S. C., Yang, T. N., Wang, Y., Chi, Z., Lee, T.Q., Chen, M.T., Cheng, C.L., Zou, J., Chang, Y. P., 2013. The Ti/Al molar ratio as a new proxy for tracing sediment transportation processes and its application in aeolian events and sea level change in East Asia. Journal of Asian Earth Sciences 73, 31-38.

Chenot, E., Deconinck, J.-F., Pucéat, E., Pellenard, P., Cuiraud, M., Jaubert, M., Jarvis, I., Thibault, N., Cocquerez, T., Bruneau, L., Razmjooei, M.J., Boussaha, M., Richard, J., Sizun, J.-P., Stemmerik, L., 2018. Continental weathering as a driver of Late Cretaceous cooling: new insights from clay mineralogy of Campanian sediments from the southern Tethyan margin to the Boreal realm. Global and Planetary Change 162, 292–312. https://doi.org/10.1016/j.gloplacha.2018.01.016

Chu, N.-C., Taylor, R.N., Chavagnac, V., Nesbitt, R.W., Boella, R.M., Milton, J.A., German, C.R., Bayon, G., Burton, K., 2002. Hf isotope ratio analysis using multi-collector inductively coupled plasma mass spectrometry: an evaluation of isobaric interference corrections. J. Anal. At. Spectrom. 17, 1567–1574. https://doi.org/10.1039/B206707B

Clauer, N., O'Neil, J.R., Bonnot-Courtois, C., Holtzapffel, T., 1990. Morphological, Chemical, and Isotopic Evidence for an Early Diagenetic Evolution of Detrital Smectite in Marine Sediments. Clays Clay Miner. 38, 33–46. https://doi.org/10.1346/CCMN.1990.0380105

Daoudi, L., 2004. Palygorskite in the uppermost Cretaceous–Eocene rocks from Marrakech High Atlas, Morocco. Journal of African Earth Sciences, Key Points on African Geology 39, 353–358. https://doi.org/10.1016/j.jafrearsci.2004.07.033

Dausmann, V., Gutjahr, M., Frank, M., Kouzmanov, K., Schaltegger, U., 2019. Experimental evidence for mineral-controlled release of radiogenic Nd, Hf and Pb isotopes from granitic rocks during progressive chemical weathering. Chemical Geology, 507, 64-84.

Dera, G., Pellenard, P., Neige, P., Deconinck, J.-F., Pucéat, E., Dommergues, J.-L., 2009. Distribution of clay minerals in Early Jurassic Peritethyan seas: Palaeoclimatic significance inferred from multiproxy comparisons. Palaeogeography, Palaeoclimatology, Palaeoecology 271, 39–51. doi: 10.1016/j.palaeo.2008.09.010.

Derry, L.A., France-Lanord, C., 1996. Neogene Himalayan weathering history and river87Sr86Sr: impact on the marine Sr record. Earth and Planetary Science Letters 142, 59–74. https://doi.org/10.1016/0012-821X(96)00091-X

Dupont-Nivet, G., Hoorn, C., Konert, M., 2003. Tibetan uplift prior to the Eocene-Oligocene climate transition: Evidence from pollen analysis of the Xining Basin. Geology 36, 987–990. https://doi.org/10.1130/G25063A.1

Engelmann de Oliveira, C.H., Jelinek, A.R., Chemale, F., Cupertino, J.A., 2016. Thermotectonic history of the southeastern Brazilian margin: Evidence from apatite fission track data of the offshore Santos Basin and continental basement. Tectonophysics 685, 21–34. https://doi.org/10.1016/j.tecto.2016.07.012

Fagel, N., André, L., Chamley, H., Debrabant, P., Jolivet, L., 1992. Clay sedimentation in the Japan Sea since the Early Miocene: influence of source-rock and hydrothermal activity. Sedimentary Geology 80, 27–40. https://doi.org/10.1016/0037-0738(92)90029-Q

Fantasia, A., Adatte, T., Spangenberg, J.E., Font, E., Duarte, L.V., Föllmi, K.B., 2019. Global versus local processes during the Pliensbachian–Toarcian transition at the Peniche GSSP, Portugal: A multi-proxy record. Earth-Science Reviews 198, 102932.

https://doi.org/10.1016/j.earscirev.2019.102932

Fernandes, L.A., Magalhães Ribeiro, C.M., 2015. Evolution and palaeoenvironment of the Bauru Basin (Upper Cretaceous, Brazil). Journal of South American Earth Sciences 61, 71–90. https://doi.org/10.1016/j.jsames.2014.11.007

Franco-Magalhaes, A.O., Hackspacher, P.C., Glasmacher, U.A., Saad, A.R., 2010. Rift to post-rift evolution of a "passive" continental margin: the Ponta Grossa Arch, SE Brazil. Int. J. Earth Sci. 99 (7), 1599–1613.

Frank, M., 2002. Radiogenic Isotopes: Tracers of Past Ocean Circulation and Erosional Input. Reviews of Geophysics 40, 1-1-1–38. https://doi.org/10.1029/2000RG000094

Freslon, N., Bayon, G., Birot, D., Bollinger, C., Barrat, J.A., 2011. Determination of rare earth elements and other trace elements (Y, Mn, Co, Cd) in seawater using Tm addition and $Mg(OH)_2$ co-precipitation. Talanta 85 (1), 582-587.

Friedrich, O., Norris, R.D., Erbacher, J., 2012. Evolution of middle to Late Cretaceous oceans—A 55 m.y. record of Earth's temperature and carbon cycle. Geology 40, 107–110. https://doi.org/10.1130/G32701.1

Gabet, E.J., Mudd, S.M., 2009. A theoretical model coupling chemical weathering rates with denudation rates. Geology 37, 151–154. https://doi.org/10.1130/G25270A.1

Gallagher, K., Brown, R., 1999. The Mesozoic denudation history of the Atlantic margins of southern Africa and southeast Brazil and the relationship to offshore sedimentation. Geological Society, London, Special Publications 153, 41–53. https://doi.org/10.1144/GSL.SP.1999.153.01.03

Garcia, A.J.V., da Rosa, A.A.S., Goldberg, K., 2005. Paleoenvironmental and paleoclimatic control on early diagenetic processes and fossil record in Cretaceous continental sandstones of Brazil. J. S. Am. Earth Sci. 19 (3), 243–258.

Garçon, M., Chauvel, C., 2014. Where is basalt in river sediments, and why does it matter? Earth and Planetary Science Letters 407, 61-69.

Goldstein, S.L., Hemming, S.H., 2003. Long lived isotopic tracers in oceanography, paleoceanography, and ice sheet dynamics. In: Elderfield, H., Turekian, K.K. 2003 (Eds.), Treatise on Geochemistry. Elsevier, New York, 453–489. http://dx.doi.org/10. 1016/B0-08-043751-6/06179-X.

Govindaraju, K., 1994. 1994 compilation of working values and sample description for 383 geostandards. Geostantards Newletter 18, special issue 1-158.

Gradstein, F.M., Ogg, J.G., Schmitz, M.D., Ogg, G.M., 2012. The Geologic Time Scale 2012. Elsevier.

Harman, R., Gallagher, K., Brown, R., Raza, A., Bizzi, L., 1998. Accelerated denudation and tectonic/geomorphic reactivation of the cratons of northeastern Brazil during the Late Cretaceous. Journal of Geophysical Research 103, 27,091– 27,105.

Hay, W. W., DeConto, R. M., Wold, C. N., Wilson, K. M., Voigt, S., Schulz, M., Wold-Rossby, A., Dullo, W.-C., Ronov, A. B., Balukhovsky, A. N., and Söding, E., 1999, Alternative global Cretaceous paleogeography. In Barrera, E., and Johnson, C. C. (Eds.), Evolution of the Cretaceous Ocean-Climate System: Boulder, Colorado. Geological Society of America Special Paper, 332 p.

Hay, W.W., Floegel, S., 2012. New thoughts about the Cretaceous climate and oceans. Earth Sci. Rev. 115, 262–272.

Huber, B.T., Hodell, D.A., Hamilton, C.P., 1995. Mid- to Late Cretaceous climate of the southern high latitudes: Stable isotopic evidence for minimal equator-to-pole thermal gradients. Geological Society of America Bulletin 107, 1164–1191.

Jochum, K. P., Weis, U., Schwager, B., Stoll, B., Wilson, S. A., Haug, G. H., Andreae, M. O., Enzweiler, J. (2016). Reference values following ISO guidelines for frequently requested rock reference materials. Geostandards and Geoanalytical Research, 40 (3), 333-350.

Kochhann, K.G.D., Lopes, F.M., Krahl, G., Aguiar, E., Fauth, G., 2014. Late cretaceous-early paleogene (Turonian to early Danian) planktic foraminifera from DSDP site 356: a biostratigraphic reappraisal Rev. Bras. Paleontol. 17 (2), 157-168.

Kumar, N., Gambôa, L. a. P., 1979. Evolution of the São Paulo Plateau (southeastern Brazilian margin) and implications for the early history of the South Atlantic. GSA Bulletin 90, 281–293. https://doi.org/10.1130/0016-7606(1979)90<281:EOTSPP>2.0.CO;2

Lugmair, G.W., Marti, K., 1977. Sm-Nd-Pu timepieces in the Angra dos Reis meteorite. Earth and Planetary Science Letters 35, 273–284. https://doi.org/10.1016/0012-821X(77)90131-5

Mantovanelli, S.S., Tassinari, C.C.G., Mahiques, M.M.D., Jovane, L., Bongiolo, E., 2018. Characterization of Nd Radiogenic Isotope Signatures in Sediments From the Southwestern Atlantic Margin. Front. Earth Sci. 6. https://doi.org/10.3389/feart.2018.00074

McConnell, R.B., 1968. Planation Surfaces in Guyana. The Geographical Journal 134, 506–520. https://doi.org/10.2307/1796379

McKenzie, N.R., Horton, B.K., Loomis, S.E., Stockli, D.F., Planavsky, N.J., Lee, C.-T.A., 2016. Continental arc volcanism as the principal driver of icehouse-greenhouse variability. Science 352, 444–447. https://doi.org/10.1126/science.aad5787

McLennan, S.M., 1993. Weathering and Global Denudation. The Journal of Geology 101, 295–303. https://doi.org/10.1086/648222

Modica, C.J., Brush, E.R., 2004. Postrift sequence stratigraphy, paleogeography, and fill history of the deep-water Santos Basin, offshore southeast Brazil. AAPG Bulletin 88, 923–945. https://doi.org/10.1306/01220403043

Moore, D.M., Reynolds, R.C., 1989. X-ray diffraction and the identification and analysis of clay minerals. X-ray diffraction and the identification and analysis of clay minerals.

Nesbitt, H.W., Young, G.M., 1982. Early Proterozoic climates and plate motions inferred from major element chemistry of lutites. Nature 299, 715–717. https://doi.org/10.1038/299715a0

Norton, K.P., Schlunegger, F., 2017. Lack of a weathering signal with increased Cenozoic erosion? Terra Nova 29, 265–272. https://doi.org/10.1111/ter.12278

O'Brien, C.L., Robinson, S.A., Pancost, R.D., Sinninghe Damsté, J.S., Schouten, S., Lunt, D.J., Alsenz, H., Bornemann, A., Bottini, C., Brassell, S.C., Farnsworth, A., Forster, A., Huber, B.T., Inglis, G.N., Jenkyns, H.C., Linnert, C., Littler, K., Markwick, P., McAnena, A., Mutterlose, J., Naafs, B.D.A., Püttmann, W., Sluijs, A., van Helmond, N.A.G.M., Vellekoop, J., Wagner, T., Wrobel, N.E., 2017. Cretaceous sea-surface temperature evolution: Constraints from TEX86 and planktonic foraminiferal oxygen isotopes. Earth-Science Reviews 172, 224–247. https://doi.org/10.1016/j.earscirev.2017.07.012

Ouhadi, V.R., Yong, R.N., 2003. Impact of clay microstructure and mass absorption coefficient on the quantitative mineral identification by XRD analysis. Applied Clay Science 23, 141-148.

Peucker-Ehrenbrink, B., Ravizza, G., 2000. The marine osmium isotope record. Terra Nova 12, 205–219. https://doi.org/10.1046/j.1365-3121.2000.00295.x

Perch-Nielsen, K., Supko, P.R., Boersma, E., Carlson R.L., Dinkelman M.G., Fodor R.V., Kumar N., McCoy F., Thiede J., Zimmermann, H.B., 1977. Site 356 : Sao Paulo

Plateau. In Supko, P.R. et al. 1977 (Eds.), Initial Reports of the Deep Sea Drilling Project. Washington, U.S. Government Printing Office, 1132 p. doi:10.2973/dsdp.proc.39.

Pletsch, T., 2001. Palaeoenvironmental implications of palygorskite clays in Eocene deep-water sediments from the western Central Atlantic. Geological Society, London, Special Publications 183, 307–316. https://doi.org/10.1144/GSL.SP.2001.183.01.15

Raymo, M.E., Ruddiman, W.F., Froelich, P.N., 1988. Influence of late Cenozoic mountain building on ocean geochemical cycles. Geology 16, 649–653. https://doi.org/10.1130/0091-7613(1988)016<0649:IOLCMB>2.3.CO;2

Robert, C., 1981. Santonian to Eocene palaeogeographic evolution of the Rio Grande Rise (South Atlantic) deduced from clay-mineralogical data (DSDP legs 3 and 39). Palaeogeography, Palaeoclimatology, Palaeoecology 33, 311–325. https://doi.org/10.1016/0031-0182(81)90024-9

Robert, C., Chamley, H., 1987. Cenozoic evolution of continental humidity and paleoenvironment, deduced from the kaolinite content of oceanic sediments. Palaeogeography, Palaeoclimatology, Palaeoecology 60, 171–187. https://doi.org/10.1016/0031-0182(87)90031-9

Royer, D.L., 2010. Fossil soils constrain ancient climate sensitivity. PNAS 107, 517–518. https://doi.org/10.1073/pnas.0913188107

Rudnick, R. L., & Fountain, D. M. (1995). Nature and composition of the continental crust: a lower crustal perspective. Reviews of geophysics 33 (3), 267-309.

Ruffell, A., McKinley, J.M., Worden, R.H., 2002.Comparison of clay mineral stratigraphy to other proxy palaeoclimate indicators in the Mesozoic of NW Europe. Philosophical Transactions of the Royal Society London A 360, 675-693.

Söderlund, U., Patchett, P.J., Vervoort, J.D., Isachsen, C.E., 2004. The 176Lu decay constant

determined by Lu–Hf and U–Pb isotope systematics of Precambrian mafic intrusions. Earth and Planetary Science Letters 219, 311–324. https://doi.org/10.1016/S0012-821X(04)00012-3

Tanaka, T., Togashi, S., Kamioka, H., Amakawa, H., Kagami, H., Hamamoto, T., Yuhara, M., Orihashi, Y., Yoneda, S., Shimizu, H., Kunimaru, T., Takahashi, K., Yanagi, T., Nakano, T., Fujimaki, H., Shinjo, R., Asahara, Y., Tanimizu, M., Dragusanu, C., 2000. JNdi-1: a neodymium isotopic reference in consistency with LaJolla neodymium. Chemical Geology 168, 279–281. https://doi.org/10.1016/S0009-2541(00)00198-4

Taylor, S.R., McLennan, S.M., 1985. The Continental Crust: Its Composition and Evolution. An Examination of the Geochemical Record Preserved in Sedimentary Rocks. Blackwell Scientific Publications, Oxford, 312 p.

Thiry, M., 2000. Palaeoclimatic interpretation of clay minerals in marine deposits : an outlook from the continental origin. Earth-Science Reviews 49, 201-221.

Vervoort, J.D., Patchett, P.J., Blichert-Toft, J., Albarède, F., 1999. Relationships between Lu–Hf and Sm–Nd isotopic systems in the global sedimentary system. Earth and Planetary Science Letters 168, 79–99. https://doi.org/10.1016/S0012-821X(99)00047-3

Weis, D., Kieffer, B., Maerschalk, C., Barling, J., Jong, J. de, Williams, G.A., Hanano, D., Pretorius, W., Mattielli, N., Scoates, J.S., Goolaerts, A., Friedman, R.M., Mahoney, J.B., 2006. High-precision isotopic characterization of USGS reference materials by TIMS and MC-ICP-MS. Geochemistry, Geophysics, Geosystems 7. https://doi.org/10.1029/2006GC001283

Weis, D., Kieffer, B., Maerschalk, C., Pretorius, W., Barling, J., 2005. High-precision Pb-Sr-Nd-Hf isotopic characterization of USGS BHVO-1 and BHVO-2 reference materials. Geochemistry, Geophysics, Geosystems 6. https://doi.org/10.1029/2004GC000852

West, A.J., Galy, A., Bickle, M., 2005. Tectonic and climatic controls on silicate weathering. Earth and Planetary Science Letters 235, 211–228. https://doi.org/10.1016/j.epsl.2005.03.020

West, A. J., 2012. Thickness of the chemical weathering zone and implications for erosional and climatic drivers of weathering and for carbon-cycle feedbacks. Geology, 40 (9), 811-814.

White, A.F., Blum, A.E., 1995. Effects of climate on chemical_ weathering in watersheds. Geochimica et Cosmochimica Acta 59, 1729–1747 https://doi.org/10.1016/0016-7037(95)00078-E

Willenbring, J. K., von Blanckenburg, F., 2010. Long-term stability of global erosion rates and weathering during late-Cenozoic cooling. Nature, 465 (7295), 211.

Zabel, M., Bickert, T., Dittert, L., & Haese, R. R. 1999. Significance of the sedimentary Al/Ti ratio as an indicator for variations in the circulation patterns of the equatorial North Atlantic. Paleoceanography 14 (6), 789-799.

Zimmermann, H.B., 1977. Clay mineral stratigraphy and distribution in the south Atlantic ocean. In Supko, P.R. et al. 1977 (Eds.), Initial Reports of the Deep Sea Drilling Project, Volume 39. Washington, U.S. Government Printing Office, 395-405.

Acknowledgments

We thank IODP for allowing us to access the material. IODP France and ANR RISE funded the project. We also thank Rémi Chassagnon of the ARCEN analysis centre of the Université de Bourgogne, Marie-Laure Rouget of the Pole Spectrométrie Océan in Brest and Philippe Telouk of the ENS Lyon for the analytical support.

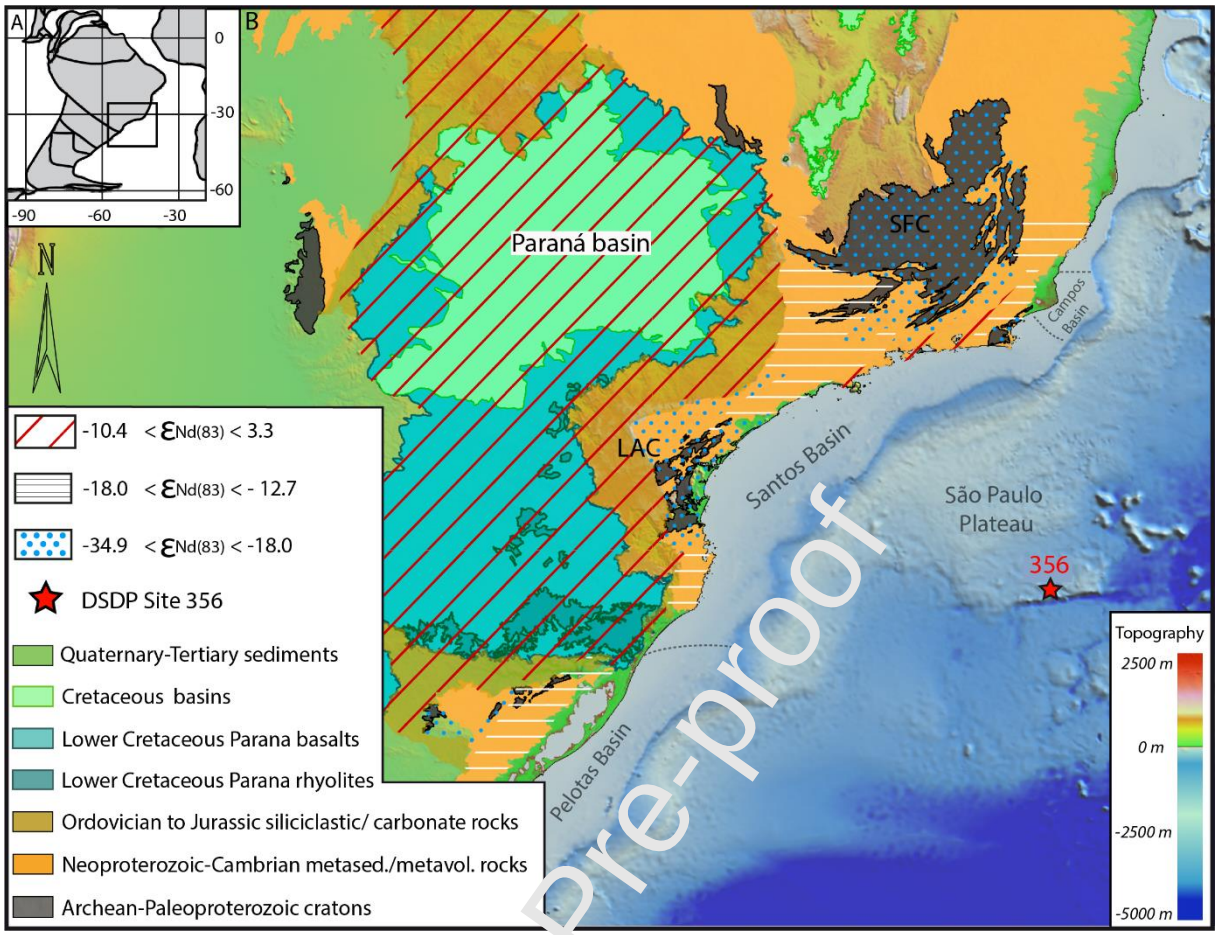

Figure 1 – A. Palaeogeographic map of the South American continent for the Campanian (80 Ma, modified from Hay et al., 1999) showing the studied zone. B. Map of the southeastern Brazilian margin with the compiled $\varepsilon_{Nd(t)}$ values from the literature and calculated at 83 Ma (Supplementary Table 2). Abbreviations : SFC = São Francisco Craton, LAC = Luis Alves Craton.

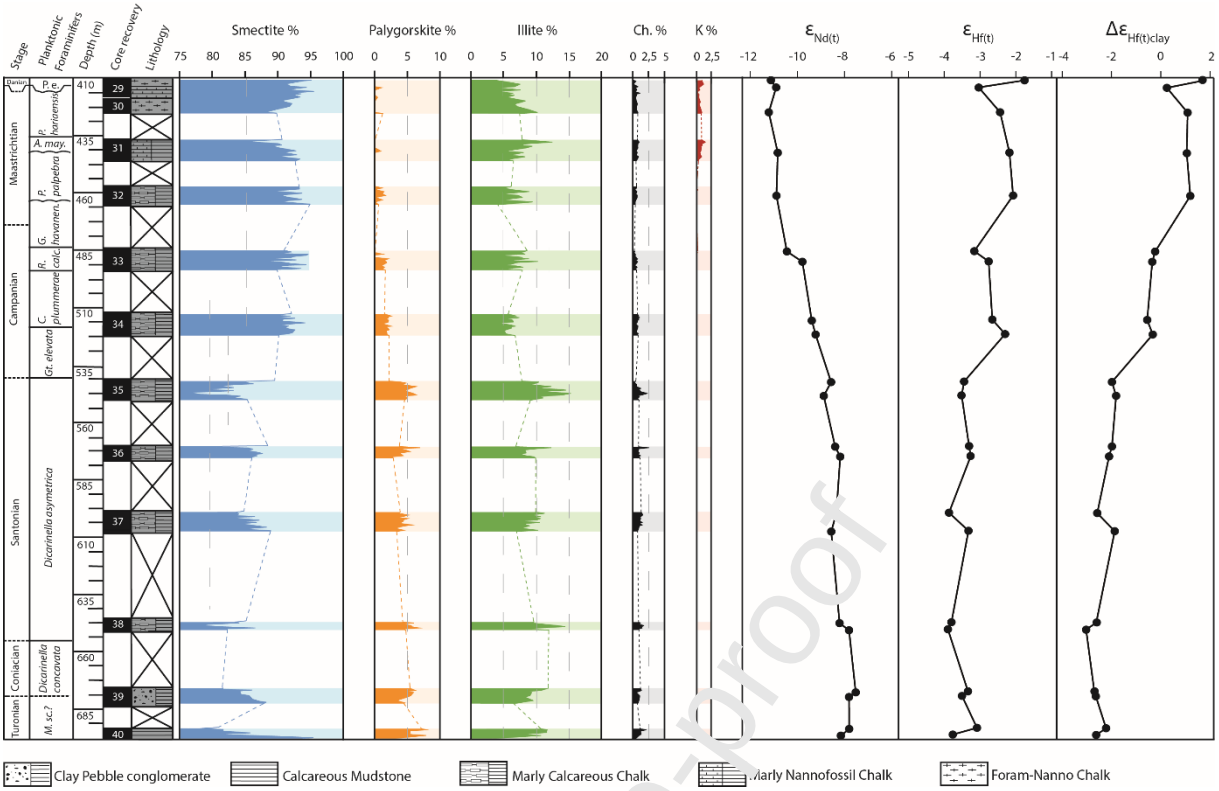

Figure 2 – Lithology, biostratigraphy, clay mineralogy, $\varepsilon_{Nd(t)}$, $\varepsilon_{Hf(t)}$ and $\Delta\varepsilon_{Hf(t)clay}$ of the Site DSDP 356. Abbreviations : P.e. = Parvularugoglobigerina eugubina ; P. har. = Pseudoguembelina fruticosa ; *A. may., Abathomphalus mayaroensis*; *P. palpebra = Pseudoguembelina palpebra*; *G. havavanen. = Globotruncanella havanensis*; *R. calc. = Radotruncana calcarata*; *C. plummerae = Contusotruncana plummerae*; *Gt. Elevata = Globotruncanita elevata*; *M. sc. = Marginotruncana schneegansi*.

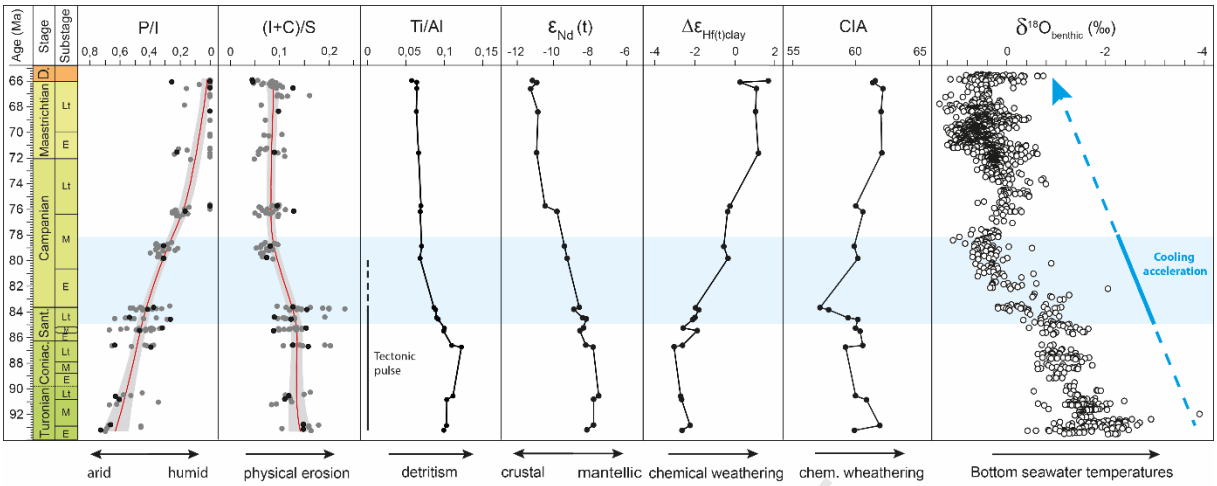

Figure 3 – Evolution of the Palygorskite/Illite (P/I), (Illite+Chlorite)/Smectite ((I+C)/S), Ti/Al, $\varepsilon_{Nd(t)}$, $\Delta\varepsilon_{Hf(t)clay}$ and CIA of the Site 356 during the Upper Cretaceous along the $\delta^{18}O_{benthic}$ from Friedrich et al., 2012. The grey dots correspond to the samples analyses by XRD only, the black dots correspond to the samples for which both geochemical and mineralogical analyses have been conducted. The white dots corresponds to the data of the literature. The cooling of the temperatures is indicated by a blue dotted arrow with the cooling acceleration marked by a bold mark and a blue banner. Smoothed curves with their 95% confidence interval have been calculated using Kernel regressions for P/I and (I+C)/S ratios, with a bandwidth of 5 m.y. representing maximal time resolution. Abbreviations : Coniac. = Coniacian, Sant. = Santonian, D. = Danian, E = Early, M = Middle, Lt = Late, chem. = chemical.

Note the increase in chemical weathering indicated by both $\Delta\varepsilon_{Hf(t)clay}$ values and CIA from the Santonian onward, that follows the main uplift phase of the margin identified by high (I+C)/S and Ti/Al ratios.

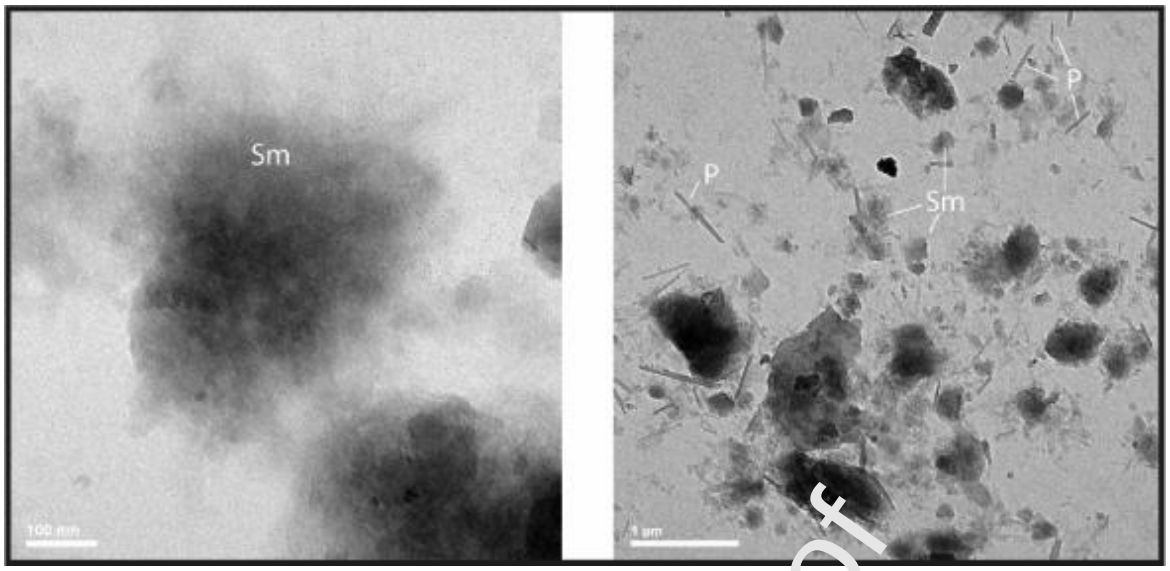

Figure 4 – Transmission electron micrographs (TEM) of detrital particles of smectite with flake shape (left, sample 29r2w89) and short fibres of detrital palygorskite with smectite particles (right, sample 37r1w83).

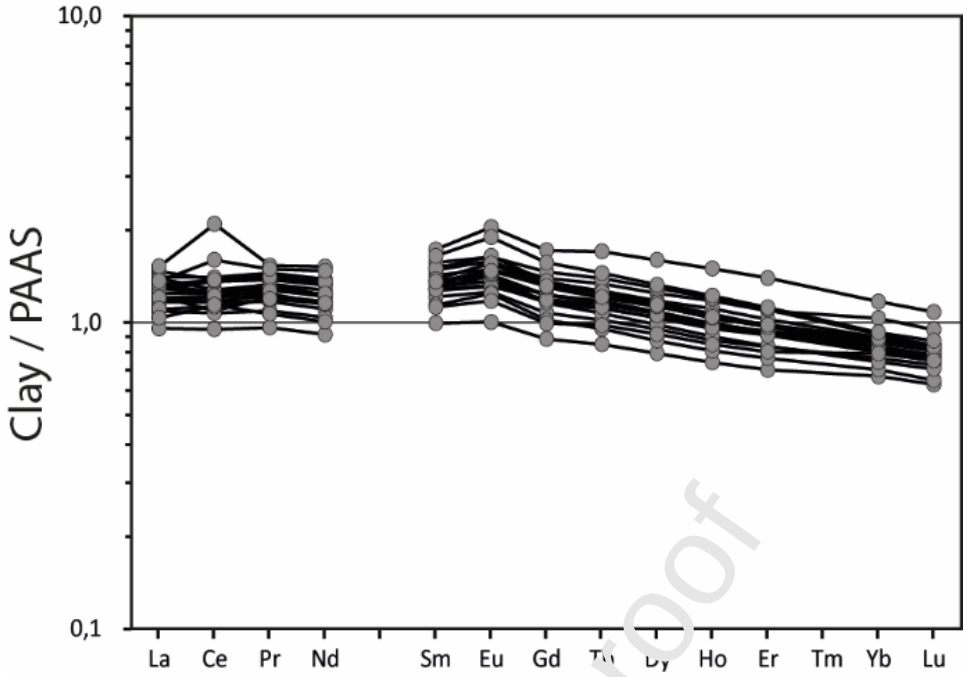

Figure 5 – Shale-normalized (PAAS; Taylor and McLennan, 1985) REE patterns for the clay fraction of the Site 356.

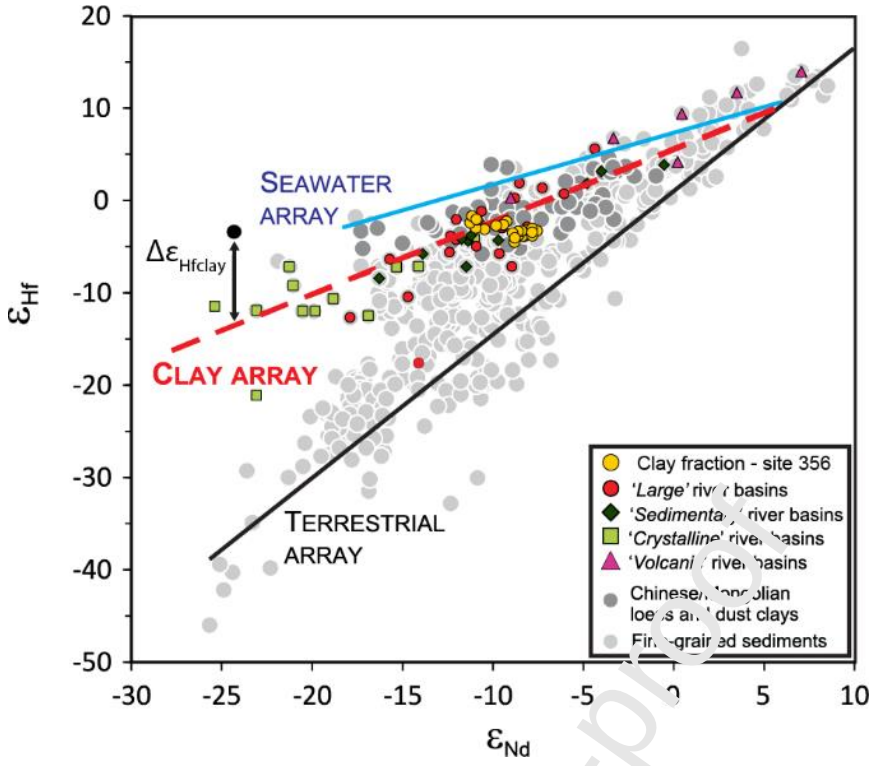

Figure 6 – Nd and Hf isotopic composition of the Site 356 plotted on the Nd and Hf composition of World River clays compilation from Bayon et al., 2016. The clay array correspond to the correlation displayed by clay ε_{Nd} and ε_{Hf} (Bayon et al., 2016). Note that the samples analyzed in this work plot along the clay array. The $\Delta\varepsilon_{Hf(t)clay}$ corresponds to the departure of a sample's clay ε_{Hf} to the clay array and reflects the degree of alteration of river clays.

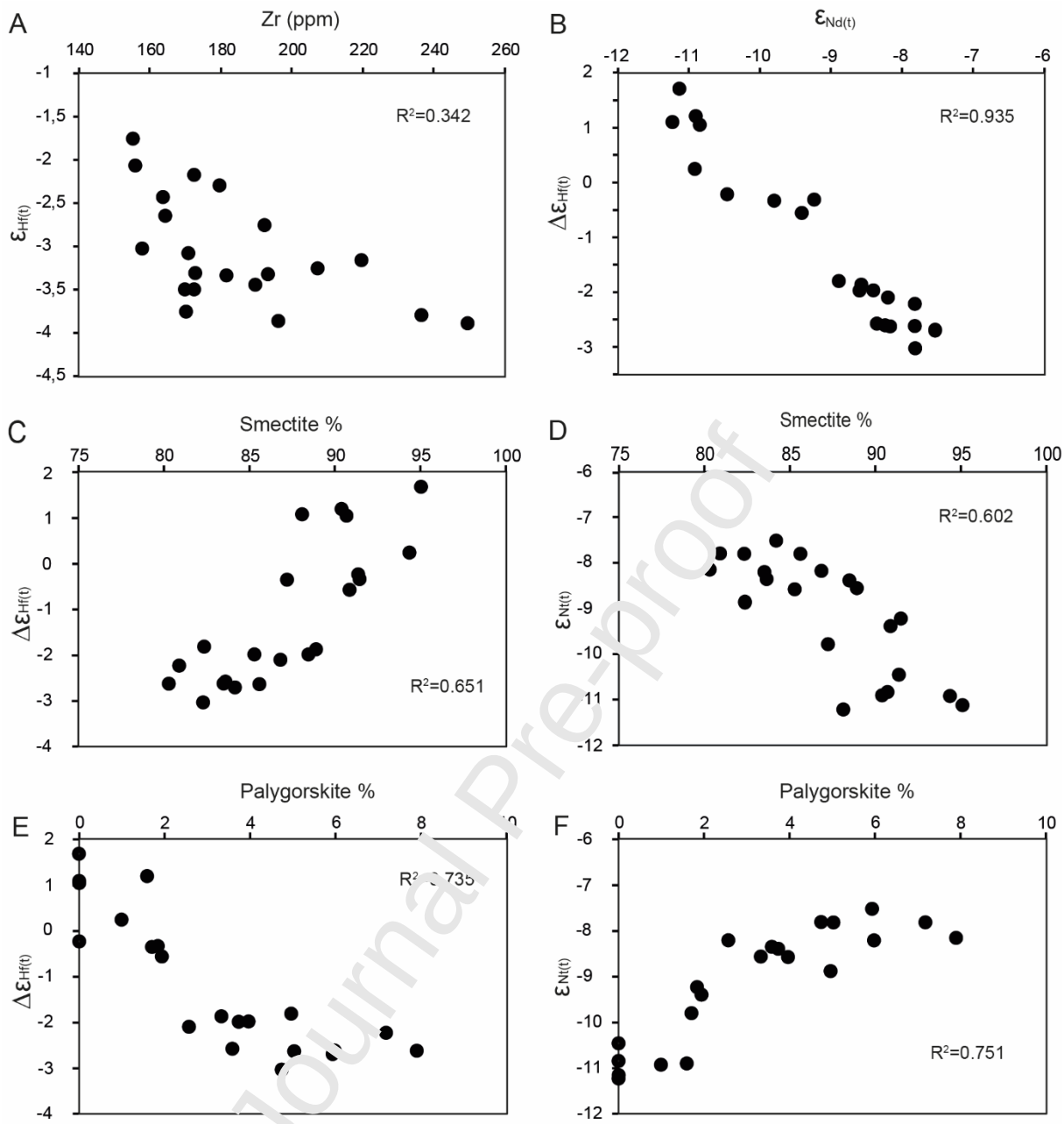

Figure 7 – A. Correlation between the $\varepsilon_{Hf=(t)}$ and Zr concentration. B. Correlation between $\Delta\varepsilon_{Hf(t)clay}$ and $\varepsilon_{Nd(t)}$. C. Correlation between $\Delta\varepsilon_{Hf(t)clay}$ and the smectite content D. Correlation between $\varepsilon_{Nd(t)}$ and the smectite content. E. Correlation between $\Delta\varepsilon_{Hf(t)clay}$ and the palygorskite content. E. Correlation between $\varepsilon_{Nd(t)}$ and the palygorskite content.

Declaration of interests

☒ The authors declare that they have no known competing financial interests or personal relationships that could have appeared to influence the work reported in this paper.

☐The authors declare the following financial interests/personal relationships which may be considered as potential competing interests:

Highlights :

First use of paired Hf-Nd isotopes to constrain continental weathering in deep-time.

Enhanced chemical weathering followed the South American margin uplift.

Rain shadow effect linked to uplift favored chemical weathering and CO2 consumption.

Tectonic uplift contributed to the late Cretacous cooling.

Enhanced continental weathering contributed to last greenhouse-to-icehouse transition.